The Astrophysical Journal Letters, 756:L38 (6pp), 2012 September 10 doi:10.1088/2041-8205/756/2/L38
© 2012. The American Astronomical Society. All rights reserved. Printed in the U.S.A.

NEAR-INFRARED IMAGING OF A $z = 6.42$ QUASAR HOST GALAXY WITH THE *HUBBLE SPACE TELESCOPE* WIDE FIELD CAMERA 3*

M. Mechtley[1], R. A. Windhorst[1,2], R. E. Ryan[3], G. Schneider[4], S. H. Cohen[1,2], R. A. Jansen[1,2], X. Fan[4], N. P. Hathi[5], W. C. Keel[6], A. M. Koekemoer[3], H. Röttgering[7], E. Scannapieco[1], D. P. Schneider[8,9], M. A. Strauss[10], and H. J. Yan[11]
[1] School of Earth and Space Exploration, Arizona State University, P.O. Box 871404, Tempe, AZ 85287, USA
[2] Department of Physics, Arizona State University, P.O. Box 871504, Tempe, AZ 85287, USA
[3] Space Telescope Science Institute, Baltimore, MD 21218, USA
[4] Steward Observatory, The University of Arizona, Tucson, AZ 85721, USA
[5] Carnegie Observatories, 813 Santa Barbara Street, Pasadena, CA 91101, USA
[6] Department of Physics and Astronomy, University of Alabama, Box 870324, Tuscaloosa, AL 35487, USA
[7] Leiden Observatory, Leiden University, P.O. Box 9513, 2300 RA, Leiden, The Netherlands
[8] Department of Astronomy and Astrophysics, The Pennsylvania State University, 525 Davey Laboratory, University Park, PA 16802, USA
[9] Institute for Gravitation and The Cosmos, The Pennsylvania State University, University Park, PA 16802, USA
[10] Princeton University Observatory, Princeton, NJ 08544, USA
[11] Department of Physics and Astronomy, The University of Missouri, 701 South College Ave, Columbia, MO 65211, USA
Received 2012 April 20; accepted 2012 August 8; published 2012 August 23

ABSTRACT

We report on deep near-infrared F125W (*J*) and F160W (*H*) *Hubble Space Telescope* Wide Field Camera 3 images of the $z = 6.42$ quasar J1148+5251 to attempt to detect rest-frame near-ultraviolet emission from the host galaxy. These observations included contemporaneous observations of a nearby star of similar near-infrared colors to measure temporal variations in the telescope and instrument point-spread function (PSF). We subtract the quasar point source using both this direct PSF and a model PSF. Using direct subtraction, we measure an upper limit for the quasar host galaxy of $m_J > 22.8$ and $m_H > 23.0$ AB mag (2σ). After subtracting our best model PSF, we measure a limiting surface brightness from 0.″3 to 0.″5 radius of $\mu_J > 23.5$ and $\mu_H > 23.7$ AB mag arcsec^{-2} (2σ). We test the ability of the model subtraction method to recover the host galaxy flux by simulating host galaxies with varying integrated magnitude, effective radius, and Sérsic index, and conducting the same analysis. These models indicate that the surface brightness limit ($\mu_J > 23.5$ AB mag arcsec^{-2}) corresponds to an integrated upper limit of $m_J > 22$–23 AB mag, consistent with the direct subtraction method. Combined with existing far-infrared observations, this gives an infrared excess log(IRX) > 1.0 and corresponding ultraviolet spectral slope $\beta > -1.2 \pm 0.2$. These values match those of most local luminous infrared galaxies, but are redder than those of almost all local star-forming galaxies and $z \simeq 6$ Lyman break galaxies.

Key words: galaxies: high-redshift – methods: observational – quasars: individual (SDSS J1148+5251)

1. INTRODUCTION

Since their discovery by Schmidt (1963), quasars have been the best and most easily observed beacons to probe the distant universe. The unification model for active galactic nuclei (AGNs; e.g., Antonucci 1993 and references therein) views quasars as unobscured active nuclei, with a supermassive black hole (SMBH) as the central powerhouse behind the dominant nonstellar continuum.

Ground-based studies (e.g., Boroson & Oke 1982; McLeod & Rieke 1994) are limited by atmospheric seeing, and show that observing the underlying stellar populations is not trivial. Targett et al. (2012) have recently imaged $z \simeq 4$ quasar host galaxies using adaptive optics with the European Southern Observatory Very Large Telescope, but these required the best seeing conditions and targets with nearby (<40 arcsec) bright stars. Studies with the *Hubble Space Telescope* (*HST*) have concentrated on quasars at $z \simeq 0.5$–3, yielding important constraints on the morphology, luminosity, and stellar populations of quasar hosts (e.g., Disney et al. 1995; McLeod & Rieke 1995; Bahcall et al. 1997; McLure et al. 1999; Ridgway et al. 2001; Hutchings et al. 2002; Dunlop et al. 2003; Peng et al. 2006; Zakamska et al. 2006).

Goto et al. (2009) and Willott et al. (2011) used ground-based telescopes to detect extended Lyα emission out to 15 kpc around the $z = 6.42$ quasar CFHQS J232908−030158. This underscores the need to observe at longer, rest-frame near-ultraviolet wavelengths if emission from the host galaxy is to be differentiated from surrounding gas.

Imaging quasar host galaxies allows one to examine how mergers, starbursts, and other changes in environment affect the central nucleus. Observations of molecular gas and the far-infrared continua of $z \simeq 6$ quasars have suggested extremely high average star formation rates of $\gtrsim 1000\ M_\odot\ \mathrm{yr}^{-1}$ (Wang et al. 2010), implying potentially luminous hosts. As many quasars are hosted in massive galaxies, imaging $z \simeq 6$ quasar hosts may reveal the properties of the most massive first galaxies. The enormous SMBH mass ($>10^9\ M_\odot$) associated with Sloan Digital Sky Survey (SDSS; York et al. 2000) quasars at $z \simeq 6$ represents a great theoretical challenge that heavily constrains possible formation methods and merger histories (Volonteri & Rees 2006; Li et al. 2007).

SDSS J114816.64+525150.3 (hereafter J1148+5251) is the best-studied member of the $z \simeq 6$ quasar population, having been extensively observed at multiple wavelengths since its discovery by Fan et al. (2003). Near-infrared spectroscopy by Willott et al. (2003) and Iwamuro et al. (2004) measured the

* Based on observations made with the NASA/ESA *Hubble Space Telescope*, which is operated by the Association of Universities for Research in Astronomy, Inc., under NASA contract NAS 5-26555. These observations are associated with Program ID 12332.

Mg II and Fe II features, estimating a mass of $3 \times 10^9\ M_\odot$ for the SMBH, an accretion rate near the Eddington limit, and an Fe II/Mg II ratio consistent with quasars at lower redshifts. Radio observations of CO lines (e.g., Walter et al. 2003; Riechers et al. 2009) indicate the presence of 2.2–2.4 $\times 10^{10}\ M_\odot$ of high-excitation molecular gas extending to $\simeq$2.5 kpc ($r = 0\farcs45$). Studies of the [C II] line at 158 μm (Maiolino et al. 2005; Walter et al. 2009) provide evidence that the quasar host galaxy is undergoing a vigorous starburst, with an estimated star formation rate density of $\simeq$1000 $M_\odot$ yr^{-1} kpc^{-2} extending over kiloparsec scales. Studies of the continuum emission at far-infrared (FIR) wavelengths indicate a warm dust component with an AGN-corrected FIR luminosity of $9.2 \times 10^{12}\ L_\odot$ (Wang et al. 2010) and corresponding dust mass of 4.2–7.0 $\times 10^8\ M_\odot$ (Bertoldi et al. 2003; Robson et al. 2004; Beelen et al. 2006). Locally, this is in the range of ultraluminous infrared galaxies (ULIRGs; galaxies with $L_{\rm FIR} > 10^{12}\ L_\odot$). Near- and mid-infrared *Spitzer Space Telescope* observations by Jiang et al. (2006) show clear evidence for prominent hot dust within the galaxy. All of these observations argue for a host galaxy with a significant stellar mass component undergoing an extreme episode of star formation.

In this Letter, we report on near-infrared imaging of J1148+5251 with the *HST* Wide Field Camera 3 (WFC3) and our methods for characterizing and subtracting the instrument and telescope point-spread function (PSF). In Section 2, we describe our near-infrared WFC3 imaging of J1148+5251 and a nearby star, used for PSF characterization. In Section 3, we describe our method for subtracting the central point source from the quasar images. We describe our simulations for assessing the reliability of our subtraction method in Section 4. Finally, in Section 5, we discuss the implications of these results and our plans for future investigation. For this Letter, we adopt a ΛCDM cosmology with $H_0 = 70.3$ km s^{-1} Mpc^{-1}, $\Omega_M = 0.271$, and $\Omega_\Lambda = 0.729$ (Komatsu et al. 2011). Unless otherwise stated, all magnitudes use the AB system (Oke 1974) and have been corrected for Galactic extinction using the map of Schlegel et al. (1998).

2. OBSERVATIONS AND DATA REDUCTION

The *HST* observations of J1148+5251 were performed on 2011 January 31 (*HST* Program ID 12332, PI: R. Windhorst) using the WFC3 IR channel with the F125W (Wide *J*) and F160W (WFC3 *H*) filters. Previous programs (e.g., Hutchings et al. 2002) found that the quality of empirical quasar point-source subtractions was significantly affected by PSF time variability. This variability is mostly due to so-called spacecraft breathing effects, i.e., thermally induced defocus of the *HST* secondary mirror due to movement of the Optical Telescope Assembly as the telescope goes into and out of Earth shadow (e.g., Hershey 1998). Examining these studies and instrument reports, we identified two primary sources of thermal variation that we expected to affect our observations—the spacecraft attitude and the orbital day–night cycle.

To minimize thermal variations due to spacecraft attitude, we constrained our PSF star to be within 5° of the target quasar, and required that the quasar and PSF star observations be collected in contiguous orbits. We further requested (and were granted) that our observations be scheduled immediately following another observation near the same celestial coordinates, thus minimizing thermal equilibration time in our first orbit. We selected the PSF star to match the quasar near-infrared colors ($(J - H) = 0.55$ Vega mag, $(H - K') = 0.72$ Vega mag) as closely as possible, to minimize differences in wavelength-dependent PSF features. Many stars with colors similar to the quasar also have SDSS spectra, since they were targeted by SDSS as high-redshift quasar candidates. We examined these spectra where available, to reject obvious spectroscopic binaries or other contaminants. After checking the resulting candidate stars for *HST* guide stars, we selected the star 2MASS J11552259+4937342 (spectral type K7, $m_J = 16.272 \pm 0.079$ Vega mag, $(J - H) = 0.488 \pm 0.158$ Vega mag, $(H - Ks) = 0.651 \pm 0.176$ Vega mag; Skrutskie et al. 2006) as our final PSF target.

Table 1
Summary of Observations

Target	Filter	Exp. Time (s)	Peak S/N
SDSS J1148+5251 (Quasar)	F125W	2478	2400
SDSS J1148+5251 (Quasar)	F160W	3646	3760
2MASS J11552259+4937342 (PSF Star)	F125W	208	1730
2MASS J11552259+4937342 (PSF Star)	F160W	335	2200

Unfortunately, there is no way to eliminate thermal variation due to the orbital day/night cycle. Thus, we constructed our orbits to ensure that we fully sampled this cycle, and that equal fractions of the final, combined quasar and PSF star images would come from any given location in orbital phase. Each quasar exposure was matched by several shorter PSF star exposures, taken at the same sub-pixel dither point at the same phase within the orbit. This phase-space sampling is summarized in the bottom panel of Figure 1. Any given detector location was never exposed beyond half-well depth in a single orbit, thus avoiding saturation or detector persistence. The quasar was observed in this pattern for three orbits in total, and the PSF star was observed for a single orbit.[12] The total exposure times for each object and filter combination are summarized in Table 1. Analysis was performed on `Multidrizzle`-combined images (Koekemoer et al. 2011) with an output pixel scale of $0\farcs065$ to achieve Nyquist sampling of the PSF core in both filters, enabling accurate spatial shifting. The cosmic-ray rejection step of `Multidrizzle` was disabled, since the WFC3 IR `MULTIACCUM` readout mode provided sufficient cosmic ray rejection.

3. POINT-SOURCE SUBTRACTION

To subtract the quasar point source, we used the program `GalFit` (Peng et al. 2010) to fit a PSF single-component model to the quasar image. We transformed the `Multidrizzle`-generated weight maps into uncertainty maps as in Dickinson et al. (2004), including the effects of correlated noise and shot noise from the quasar, and supplied these to `GalFit` as the pixel-to-pixel uncertainty ("sigma") image. We then subtracted the best-fit model from the original image and inspected the residual.

We first attempted this subtraction using the image of our PSF star as the model PSF. The results are shown in Figure 1. We measured the residuals using a $0\farcs5$ radius aperture, obtaining upper limits of $m_J > 22.8$ mag and $m_H > 23.0$ mag (2σ). This includes the total noise contribution from both the quasar and the empirical PSF, measured by scaling the PSF uncertainty

[12] An additional PSF star, 2MASS J11403198+5620582, was also observed for a single orbit to allow for inter-orbit interpolation of the PSF measurement. This observation suffered from a poor guide star acquisition and was unusable.

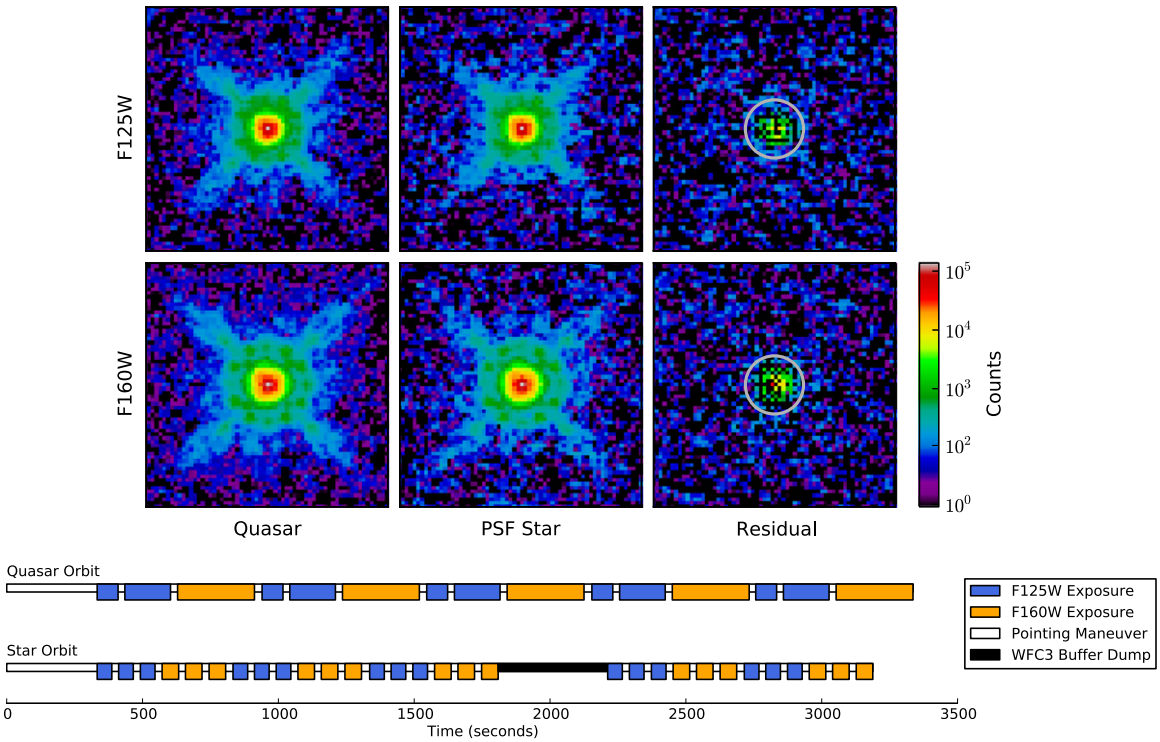

Figure 1. Empirical PSF subtraction. Left panels: `Multidrizzle`-combined F125W (J, top) and F160W (H, bottom) WFC3 images of J1148+5251 after sky subtraction. Pixels are 0.″065. Middle panels: scaled and shifted PSF star, as fit by `GalFit`. Right panels: fit residuals, showing a net positive residual flux, but high noise. We measured the integrated residual flux using a 0.″5 radius aperture (gray circle), obtaining upper limits of $m_J > 22.8$ mag and $m_H > 23.0$ mag (2σ). All images are displayed with the same logarithmic stretch. Bottom panels: PSF star and one quasar orbit, highlighting the relative phasing of corresponding dither points to compensate for spacecraft breathing. Exact phase matches are not possible due to buffer dumps and specific readout sequences. Corresponding dither points were centered at similar positions on the detector to account for field-dependent PSF variability.

map by the same factor as in the fit, and adding it in quadrature to the quasar uncertainty map. The noise contribution from the subtracted PSF is comparable to that of the quasar since the two images have comparable signal-to-noise ratio (S/N; see Table 1), which leads to cosmetic defects (holes) in the subtraction, despite the net positive residual.

We also generated a `TinyTim`[13] (Krist et al. 2011) model of the PSF, which we calibrated to the PSF star observations. A 5× spatially oversampled `TinyTim` model was generated for each WFC3 exposure to allow for subpixel shifting. We used the spectrum of J1148+5251 obtained by Iwamuro et al. (2004) as our model spectrum. We used the *HST* Focus Model[14] (Cox & Niemi 2011) to estimate the secondary mirror despace for each exposure, and included the field-dependent coma and astigmatism measurements built into `TinyTim`. The individual *HST* detectors have different mean focus offsets in the Focus Model, but the offset for the WFC3 IR channel has not been characterized. We therefore allowed the mean $Z4$ Zernike coefficient in `TinyTim` (R_2^0 in the original formulation of Zernike 1934) to float as a free parameter in our optimization, adding this single mean value to the Focus Model estimate for each exposure. These models for individual exposures were then combined, weighted by exposure time, to produce a composite PSF for each `Multidrizzle`-combined science image. `GalFit` also accepts a pixel response convolution kernel for oversampled PSFs. We generated this quantity in a similar manner, by drizzling copies of the empirical WFC3 pixel response convolution kernel (modeling inter-pixel capacitance and jitter; see Hartig 2008) using the same shifts applied to the real images.

The result of the `TinyTim` PSF subtraction, with a significantly reduced noise floor compared to the direct subtraction, is shown in Figure 2. No host galaxy is detected, to a limiting surface brightness from $r = 0.''3$ to $0.''5$ radius of $\mu_J > 23.5$ and $\mu_H > 23.7$ mag arcsec^{-2} (2σ). The inner $0.''3$ was excluded from the fit, as the best-fit `TinyTim` models produce PSF cores that are consistently narrower than those observed. Visible residuals (diffraction spikes and spots) are also seen when subtracting this model from the PSF star observations.

4. HOST GALAXY SIMULATIONS

Having established no host galaxy detection using the `TinyTim` PSF, we sought to quantify this subtraction method's ability to recover the host galaxy flux as a function of host galaxy parameters. To do so, we used `GalFit` to simulate a point source along with a Sérsic profile host galaxy, with total flux adding up to $m_J = 19.1$ mag, the measured flux in F125W. This simulated image contained no noise, so we added both shot noise from the object and a Gaussian noise field drizzled in the same manner as the real quasar image, to match its correlated noise properties. We then performed the same analysis that we used on the real quasar image, using `GalFit` to subtract a `TinyTim`-generated point source and measuring the surface brightness from $r = 0.''3$ to $0.''5$ in the residual image.

We ran a grid of 256 models using this technique, varying the total integrated flux of the host galaxy from $m_J = 20$ to 26 mag, the effective radius from $r_e = 0.''1$ to $0.''9$, and Sérsic indexes $n = 1.0$ and 4.0. The magnitude range represents host galaxies

[13] http://www.stsci.edu/hst/observatory/focus/TinyTim
[14] http://www.stsci.edu/hst/observatory/focus/FocusModel

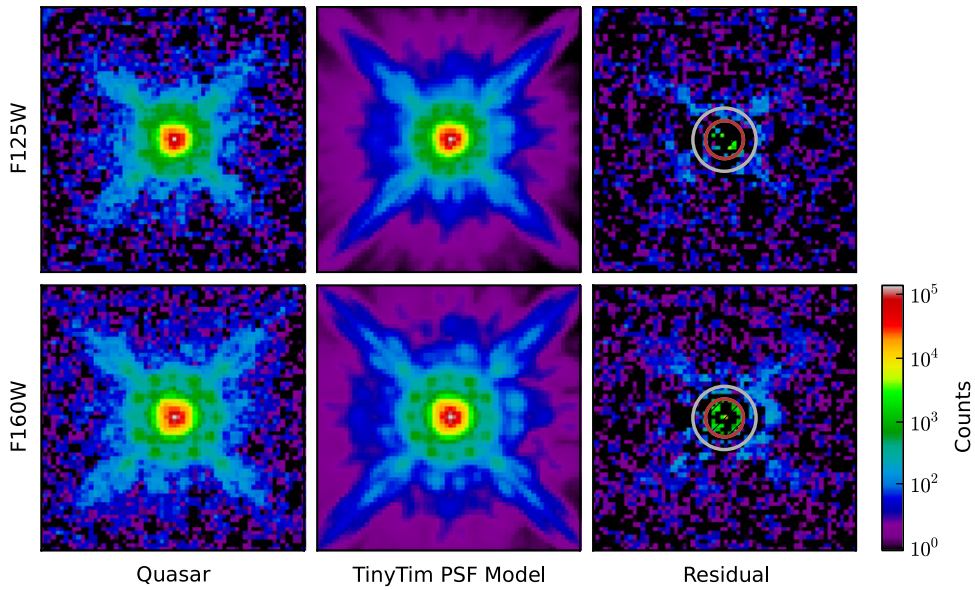

Figure 2. Model PSF subtraction. Left panels: `Multidrizzle`-combined F125W (J, top) and F160W (H, bottom) WFC3 images of J1148+5251. Middle panels: `TinyTim` models of the quasar point source, constructed by optimizing parameters for the PSF star observations, then scaled and shifted by `GalFit`. Right panels: fit residuals, showing no significant detection of the underlying galaxy beyond 0.″3 radius. The oversubtracted flux in the central 0.″3 (inner circle) occurs because the best-fit model PSFs have more power in the central peak than the observations and is also seen in residuals when modeling the PSF star. This region was excluded from the fit. The noise floor in the residual panel is 40% that of the residual panel in Figure 1. From $r = 0.''3$ to $0.''5$ (between inner and outer circles) we measure a limiting surface brightness of $\mu_J > 23.5$ and $\mu_H > 23.7$ mag arcsec^{-2} (2σ). The noise in the quasar image and uncertainties in the PSF model contribute roughly equally within this region. Visible residuals (diffraction spikes and spots) are also seen when subtracting this model from the PSF star image.

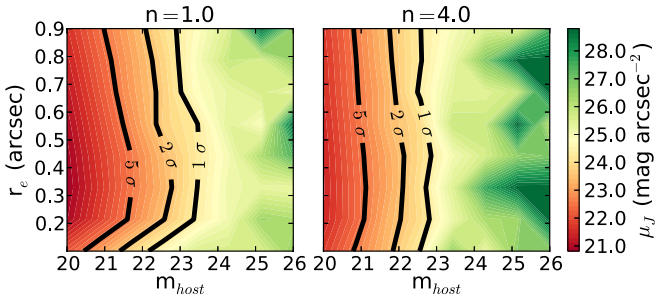

Figure 3. PSF subtraction on simulated host galaxies. Surface brightness predicted from $r = 0.''3$ to $0.''5$ as a function of simulated host galaxy parameters. The simulated observation is approximated as a PSF component along with a Sérsic profile, with total flux adding up to the observed m_J from our WFC3 image. The integrated magnitude ($m_{\rm host}$), effective radius (r_e), and Sérsic index ($n = 1.0$, left panels and $n = 4.0$, right panels) of the Sérsic profile are varied with each model. The 1σ, 2σ, and 5σ detection significance levels are plotted as black lines. The measured surface brightness reaches the 2σ limit ($\mu_J > 23.5$ mag arcsec^{-2}) for a host galaxy of $m_J > 22$–23 mag, depending upon Sérsic index and effective radius.

with luminosities from $\simeq 1/2$ to $1/500$ of the total quasar luminosity. Fainter host galaxies than this are undetectable due to shot noise from the point source. The range in effective radius corresponds to $r_e \simeq 0.6$–5.0 kpc at $z = 6.42$.

Figure 3 summarizes the results of these simulations, plotting the measured surface brightness from $r = 0.''3$ to $0.''5$ and contours representing the 1σ, 2σ, and 5σ detection limits. Inspecting the residuals of these model subtractions, we also found that bright ($m_J < 22.5$ mag), compact ($r_e < 0.''3$) host galaxies would cause the method to significantly oversubtract the PSF. This would show negative residuals from the diffraction spikes, which are not seen in Figure 2.

The model surface brightness from $r = 0.''3$ to $0.''5$ reaches the 2σ upper limit of $\mu_J > 23.5$ mag arcsec^{-2} for a host galaxy of $m_J > 22$–23 mag, depending upon Sérsic index and effective radius.

5. DISCUSSION

We have performed point-source subtraction on the $z = 6.42$ quasar J1148+5251, with both empirical and modeled PSFs. Using direct subtraction, we measure an upper limit of $m_J > 22.8$ mag and $m_H > 23.0$ mag (2σ). With the modeled PSF subtraction, we measure a limiting surface brightness measured from $0.''3$ to $0.''5$ of $\mu_J > 23.5$ mag arcsec^{-2} and $\mu_H > 23.7$ mag arcsec^{-2} (2σ). Performing the same subtraction method on simulated quasars, we found that this surface brightness limit corresponds to a host galaxy of $m_J > 22$–23 mag, consistent with the direct subtraction limit.

Using the direct subtraction limits, the upper limits on the rest-frame monochromatic luminosity (λL_λ) at 1700 Å and 2200 Å are $L_{1700} < 8.4 \times 10^{11}\ L_\odot$ and $L_{2200} < 5.4 \times 10^{11}\ L_\odot$, assuming a flat spectrum within each band when applying the K-correction (Oke & Sandage 1968). This is comparable to the most luminous Lyman break galaxies at $z \simeq 2$–3 (Hoopes et al. 2007).

Using our upper limits and Equation (1) from Kennicutt (1998), which relates L_ν to star formation rate, we estimate a star formation rate of SFR < 210–250 $M_\odot$ yr^{-1}. This estimate ignores dust attenuation and assumes a continuous star formation rate over 10^8 years or longer. A younger population would decrease this upper limit, while dust would allow for a higher (absorption-corrected) rate. The star formation rate estimated from the AGN-corrected FIR luminosity by Wang et al. (2010) is 2380 $M_\odot$ yr^{-1}. Since J1148+5251 would be classified as a ULIRG locally, this discrepancy is likely due to significant UV absorption by dust.

We can constrain the infrared excess (IRX) of the host galaxy, defined as the infrared to far-ultraviolet (FUV) luminosity ratio $L_{\rm IR}/L_{\rm FUV}$ (e.g., Howell et al. 2010), usually expressed

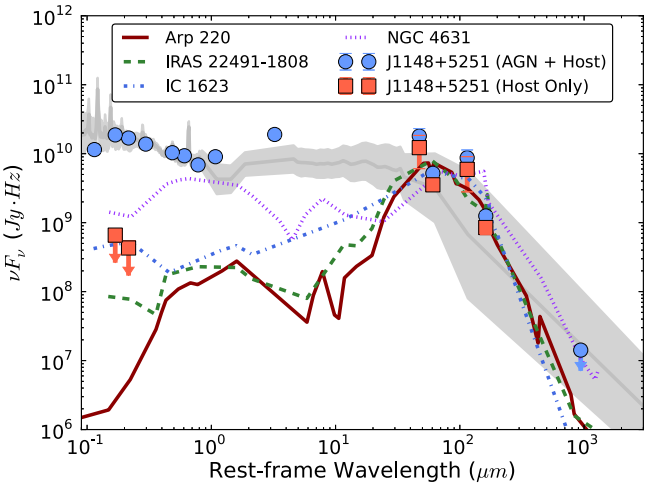

Figure 4. Comparison of broadband photometry for J1148+5251 to local galaxies. Blue circles are broadband (quasar and host) photometry of J1148+5251 taken from Fan et al. (2003), Iwamuro et al. (2004), Jiang et al. (2006), Beelen et al. (2006), Robson et al. (2004), and Bertoldi et al. (2003). Red squares show our upper limits for the host galaxy flux at 1700 Å and 2200 Å, and the AGN-corrected FIR measurements from Wang et al. (2010). The light gray spectrum is the average radio-quiet quasar spectrum of Shang et al. (2011), normalized to J1148+5251 from 0.1 to 1 μm. The dotted purple SED is NGC 4631, a local spiral with log(IRX) < 1.0. Other SEDs are those of the local LIRGs Arp 220 (solid red, log(IRX) $= 3.423$), IRAS 22491−1808 (dashed green, log(IRX) $= 2.198$), and IC 1623 (dot-dashed blue, log(IRX) $= 1.379$), representing high, average, and low IRX LIRGs, respectively (Howell et al. 2010). The local galaxy SEDs have been normalized to match the AGN-corrected emission of J1148+5251 between rest-frame 40 and 200 μm. Our constraint of log(IRX) > 1.0 (and the 2200 Å flux limit) matches most local LIRGs, but is greater than almost all local star-forming galaxies and high-redshift Lyman break galaxies (Howell et al. 2010; Overzier et al. 2011).

in logarithmic units. Using our upper limit for L_{1700} and an AGN-corrected infrared luminosity $L_{\rm IR} = 9.2 \times 10^{12}\ L_\odot$ (Wang et al. 2010), we calculate log(IRX) > 1.0, consistent with local luminous infrared galaxies (LIRGs) and ULIRGs (Howell et al. 2010), but greater than local starburst galaxies and high-redshift Lyman break galaxies (Overzier et al. 2011).

Figure 4 plots broadband measurements for J1148+5251, as well as our upper limits for the host galaxy flux at 1700 Å and 2200 Å and the AGN-corrected FIR measurements of Wang et al. (2010). Also plotted are the spectral energy distributions (SEDs) of four local galaxy systems—three LIRGs (Arp 220, IRAS 22491−1808, and IC 1623), representing the range in IRX from Howell et al. (2010), and the star-forming spiral NGC 4631, representing a galaxy with log(IRX) < 1.0, which is thus excluded as a potential host. Photometric points for the local galaxies are taken from NED[15] and the SEDs have been normalized to match the AGN-corrected emission of J1148+5251 between 40 and 200 μm.

We estimate $A_{\rm FUV} > 2.1$ mag of UV absorption using the relation between the IRX flux ratio and $A_{\rm FUV}$ (e.g., Overzier et al. 2011, Equation (1)). Using the empirical relation ${\rm IRX}_{M99,{\rm inner}}$ ($A_{\rm FUV} = 4.54 + 2.07\beta \pm 0.4$) from Overzier et al. (2011), we obtain a limit of $\beta > -1.2 \pm 0.2$. This matches local (U)LIRGs (Howell et al. 2010), but is redder than almost all local star-forming galaxies and $z \simeq 6$ Lyman break galaxies (Overzier et al. 2011; Bouwens et al. 2012).

The `TinyTim`-based subtraction may be improved in the future with more accurate WFC3 IR PSFs. Since uncertainties introduced by the PSF model scale with PSF brightness, our further WFC3 observations will target quasars where the contrast ratio between point source and host galaxy is expected to be smaller, such as optically faint $z \simeq 6$ quasars with large FIR luminosities. The *James Webb Space Telescope* will enable us to use the PSF subtraction method at rest-frame ultraviolet and optical wavelengths with better-sampled empirical PSFs in a more stable thermal environment.

[15] The NASA/IPAC Extragalactic Database (NED) is operated by the Jet Propulsion Laboratory, California Institute of Technology, under contract with NASA.

Special thanks are due to K. Long, J. MacKenty, and A. Roman at STScI for their advice and expertise when planning the observations, and the anonymous referee for very useful suggestions. We are grateful to J. Krist and C. Peng for the public availability of `TinyTim` and `GalFit`, respectively. This research has made use of the SIMBAD database, operated at CDS, Strasbourg, France. Support for this *HST* program was provided by NASA through grant GO-12332.*.A from the Space Telescope Science Institute, which is operated by the Association of Universities for Research in Astronomy, Inc., under NASA Contract NAS 5−26555. We owe a deep debt of gratitude to the entire WFC3 instrument team and the astronauts of STS-125 for this marvelous instrument on *HST*.

REFERENCES

Antonucci, R. 1993, ARA&A, 31, 473
Bahcall, J. N., Kirhakos, S., Saxe, D. H., & Schneider, D. P. 1997, ApJ, 479, 642
Beelen, A., Cox, P., Benford, D. J., et al. 2006, ApJ, 642, 694
Bertoldi, F., Carilli, C. L., Cox, P., et al. 2003, A&A, 406, 55
Boroson, T. A., & Oke, J. B. 1982, Nature, 296, 397
Bouwens, R. J., Illingworth, G. D., Oesch, P. A., et al. 2012, ApJ, 754, 83
Cox, C., & Niemi, S.-M. 2011, Instrument Science Report, TEL 2011-01 (Baltimore, MD: STScI)
Dickinson, M., Stern, D., Giavalisco, M., et al. 2004, ApJ, 600, L99
Disney, M. J., Boyce, P. J., Blades, J. C., et al. 1995, Nature, 376, 150
Dunlop, J. S., McLure, R. J., Kukula, M. J., et al. 2003, MNRAS, 340, 1095
Fan, X., Strauss, M. A., Schneider, D. P., et al. 2003, AJ, 125, 1649
Goto, T., Utsumi, Y., Furusawa, H., Miyazaki, S., & Komiyama, Y. 2009, MNRAS, 400, 843
Hartig, G. F. 2008, Instrument Science Report, SESD-08-41 (Baltimore, MD: STScI)
Hershey, J. L. 1997, Instrument Science Report, SESD-97-01 (Baltimore, MD: STScI)
Hoopes, C. G., Heckman, T. M., Salim, S., et al. 2007, ApJS, 173, 441
Howell, J. H., Armus, L., Mazzarella, J. M., et al. 2010, ApJ, 715, 572
Hutchings, J. B., Frenette, D., Hanisch, R., et al. 2002, AJ, 123, 2936
Iwamuro, F., Masahiko, M., Eto, S., et al. 2004, ApJ, 614, 69
Jiang, L., Fan, X., Hines, D. C., et al. 2006, AJ, 132, 2127
Kennicutt, R. C., Jr. 1998, ARA&A, 36, 189
Koekemoer, A. M., Faber, S. M., Ferguson, H. C., et al. 2011, ApJS, 197, 36
Komatsu, E., Smith, K. M., Dunkley, J., et al. 2011, ApJS, 192, 18
Krist, J. E., Hook, R. N., & Stoehr, F. 2011, Proc. SPIE, 8127, 81270J-1
Li, Y., Hernquist, L., Robertson, B., et al. 2007, ApJ, 665, 187L
Maiolino, R., Cox, P., Caselli, P., et al. 2005, A&A, 440, 51
McLeod, K., & Rieke, G. 1994, ApJ, 420, 58
McLeod, K., & Rieke, G. 1995, ApJ, 454, 77
McLure, R. J., Kukula, M. J., Dunlop, J. S., et al. 1999, MNRAS, 308, 377
Oke, J. B. 1974, ApJS, 27, 21
Oke, J. B., & Sandage, A. 1968, ApJ, 154, 210
Overzier, R. A., Heckman, T. M., Wang, J., et al. 2011, ApJ, 726, L7
Peng, C. Y., Ho, L. C., Impey, C. D., & Rix, H.-W. 2010, AJ, 139, 2097
Peng, C. Y., Impey, C. D., Rix, H.-W., et al. 2006, ApJ, 649, 616
Ridgway, S. E., Heckman, T. M., Calzetti, D., & Lehnert, M. 2001, ApJ, 550, 122
Riechers, D. A., Walter, F., Bertoldi, F., et al. 2009, ApJ, 703, 1338
Robson, I., Priddey, R. S., Isaak, K. G., & McMahon, R. G. 2004, MNRAS, 351, L29
Schlegel, D. J., Finkbeiner, D. P., & Davis, M. 1998, ApJ, 500, 525
Schmidt, M. 1963, Nature, 197, 1040
Shang, Z., Brotherton, M. S., Wills, B. J., et al. 2011, ApJS, 196, 2
Skrutskie, M. F., Cutri, R. M., Stiening, R., et al. 2006, AJ, 131, 1163

Targett, T. A., Dunlop, J. S., & McLure, R. J. 2012, MNRAS, 420, 3621
Volonteri, M., & Rees, M. J. 2006, ApJ, 650, 669
Walter, F., Bertoldi, F., Carilli, C., et al. 2003, Nature, 424, 406
Walter, F., Riechers, D., Cox, P., et al. 2009, Nature, 457, 699
Wang, R., Carilli, C. L., Neri, R., et al. 2010, ApJ, 714, 699
Willott, C. J., Chet, S., Bergeron, J., & Hutchings, J. B. 2011, AJ, 142, 186
Willott, C. J., McLure, R. J., & Jarvis, M. J. 2003, ApJ, 587, 15
York, D. G., Adelman, J., Anderson, J. E., Jr., et al. 2000, AJ, 120, 1579
Zakamska, N. L., Strauss, M. A., Krolik, J. H., et al. 2006, AJ, 132, 1496
Zernike, F. 1934, MNRAS, 94, 377